Spatially-Resolved Photoluminescence of Monolayer MoS₂ under Controlled Environment for Ambient Optoelectronic Applications

Blake Birmingham,[†,‡] Jiangtan Yuan,[§] Matthias Filez,[⊥] Donglong Fu,[⊥] Jonathan Hu,[∥] Jun Lou,[§] Marlan O. Scully,[‡] Bert M. Weckhuysen,[⊥] and Zhenrong Zhang*[†]

[†]Department of Physics, Baylor University, Waco, Texas 76798, United States
[‡]Institute for Quantum Science and Engineering, Texas A&M University, College Station, Texas 77843, United States
[§]Department of Materials Science and NanoEngineering, Rice University, Houston, Texas 77005, United States
[⊥]Inorganic Chemistry and Catalysis group, Debye Institute for Nanomaterials Science, Utrecht University, Universiteitsweg 99, 3584 CG Utrecht, The Netherlands
[∥]Department of Electrical and Computer Engineering, Baylor University, Waco, Texas 76798, United States

Ⓢ Supporting Information
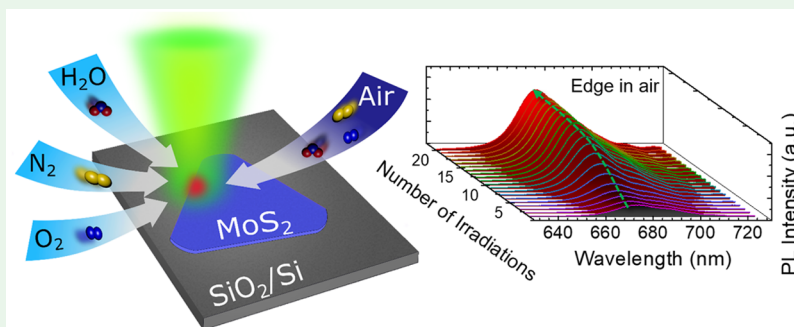
ABSTRACT: Monolayer (ML) MoS₂ has become a very promising two-dimensional material for photorelated applications, potentially serving as the basis for an ultrathin photodetector, switching device, or transistors because of its strong interaction with light in ambient conditions. Establishing the impact of individual ambient gas components on the optical properties of MoS₂ is a necessary step toward application development. By using *in situ* Raman microspectroscopy with an environment-controlled reaction cell, the photoluminescence (PL) intensity of chemical vapor deposition (CVD)-grown MoS₂ MLs is monitored at different intralayer locations under ambient and controlled gas environments, such as N₂, O₂, and H₂O. This new approach enables us to monitor the optical properties of MoS₂ at different locations on the flakes and separate the role of photoreaction of various gases during laser irradiation. Upon mild photoirradiation in ambient conditions, the PL intensity in the interior of the ML MoS₂ flakes remains unchanged, while the PL intensity at the edge region increases drastically. Photoirradiation in controlled gas environments reveals that O₂ is necessary to increase the PL intensity at the MoS₂ flake edges, attributed to the charge transfer of chemisorbed O₂. N₂ or H₂O and N₂ environments induce decreasing PL intensity upon repetitive laser irradiation. However, the H₂O and O₂ gas mixture, a combination designed to mimic ambient conditions, is necessary to maintain the PL intensity at the interior of the ML MoS₂ flakes. Our study demonstrates that photoreactions with the gaseous environment on the MoS₂ ML flakes should be taken into consideration even upon mild photoirradiation because they strongly impact the flakes' optical properties.

KEYWORDS: *monolayer molybdenum disulfide, photoluminescence, chemical doping, in situ Raman microspectroscopy, photoreaction*

INTRODUCTION

MoS₂ has a variety of potential applications including photovoltaics, energy storage, optoelectronics, and catalysis.[1−3] The chemical, optical, and electrical properties of MoS₂ in these applications are correlated and closely related to its nanoscale structural heterogeneity. For example, defects are active sites for photocatalytic and electrocatalytic processes and mediate photochemical, electrochemical, and chemical processes, which, in turn, modify the MoS₂ optoelectronic properties.[4−6] The performance of ideal MoS₂ devices could change because of laser-induced photoreactions under normal operation conditions, i.e., low-laser-power photoirradiation in ambient conditions. Therefore, correlating the structural heterogeneity, photochemistry, and optical properties of

MoS$_2$ during photoirradiation in ambient environments is critical to its various applications.

The optical properties of two-dimensional materials have been shown to be influenced by molecular interactions. The optical properties of chemical vapor deposition (CVD)-grown and mechanically exfoliated MoS$_2$ monolayers (MLs) have been previously modified via chemical treatment and doping.[7−10] The interaction of molecules with MoS$_2$ could enhance the efficiency of light−matter interactions for optoelectronic devices including low-power transistors, sensitive photodetectors, light-emitting diodes, etc.[7−10] Photoirradiation could modulate the photoluminescence (PL) of two-dimensional transition-metal dichalcogenides. Irradiating WS$_2$ surfaces with varied laser power in both air and vacuum environments was shown to optically modify the PL in WS$_2$ MLs such that the emission is from either the neutral exciton or the charged exciton (trion) state.[11] Their results suggest that the change is mitigated by surface reactions in the ambient environment. Recently, PL loss was observed on ML WS$_2$ flakes after they were briefly exposed to relatively high laser exposure under normal humid atmosphere due to H$_2$O intercalation close to the edges and defects.[12] On vacuum-annealed MoS$_2$ physisorption and chemisorption of O$_2$ and H$_2$O can significantly increase the emission efficiency.[13,14] No such effect was observed with the inert gases Ar and N$_2$. Enhancement of the PL was observed at the defect sites created by high-temperature annealing in vacuum. Recently, photoreaction on ML MoS$_2$ during high-power-laser irradiation has been studied in air and vacuum.[6] Changes in PL in ambient conditions are associated with structural damage and oxygen adsorption on the sample. However, the role of the various constituents of ambient gas during photoirradiation is not clear. The impact of the chemical reactivity of different structural areas on MoS$_2$ flakes, e.g., the interior and metallic edge, on the optical properties of MoS$_2$ during photoirradiation has yet to be understood spatially.[15] This understanding is essential for optimizing MoS$_2$ electronic and photovoltaic devices, where edge defects in large-area heterostructures can lead to interlayer leakage or unwanted exciton recombination.[16−19] In addition, laser-induced modulations of PL need to be balanced with the laser damage.

In this work, to directly correlate the structure−functionality relationship of MoS$_2$ during laser irradiation, we employed in situ Raman microspectroscopy equipped with an environment-controllable cell (see Scheme 1). The relationship between the photoreaction in various gases on ML MoS$_2$ flakes and the PL of the interior and edge of the flake has been studied. This new approach enables us to monitor the optical properties of MoS$_2$ at different locations on the flakes and separates the role of photoreaction to various gases during laser irradiation. It also allows us to simulate the effect of the ambient environment by varying the gas components. The results show that there are photoinduced reactions of molecules (O$_2$ and H$_2$O) with the MoS$_2$ ML under ambient conditions and the reaction strongly affects the PL of MoS$_2$. PL mapping of the flakes shows that the photoreaction depends on the spatial location. The PL of the edge region of the MoS$_2$ ML flakes changes dramatically under irradiation in ambient environments due to photoreactions at the edge region, while the PL of the interior of the ML stays almost unchanged under mild irradiation power.

■ RESULTS

Figure 1 depicts the change of the PL intensity of ML MoS$_2$ with laser irradiation in air at ambient temperature. Figure 1a is a typical example of a PL map taken over an entire MoS$_2$ flake (Figure 1a, inset). The high PL intensity from the ML (Figure 1a,e) in comparison to the low PL intensity from the bilayer at the center of the flake confirms that the MoS$_2$ flake is a ML with a bilayer center.[17] The separation (22.1 cm^{-1}) of the A$_{1g}$ and E$^1_{2g}$ Raman modes (Figure 1f) is consistent with previous reports for CVD-grown ML MoS$_2$.[10,15,20,21] This separation is larger than that of the exfoliated ML MoS$_2$ due to intrinsic strain. Atomic force microscopy (AFM) measurements (Figure S1) further confirm the ML.

The interior of the ML shows much higher PL intensity than the edge region of the flake (Figure 1a). Negligible PL was observed on the Si substrate as expected. The low PL intensity at the edge region is observed in almost all of the measurements taken on our samples, which is consistent with the previously reported PL maps measured on CVD-grown MoS$_2$ flakes using scanning near-field optical microscopy (SNOM).[22] Higher PL intensity from the edge region has been reported previously for MoS$_2$ flakes prepared under different synthetic conditions.[6,15]

Figure 1b shows an optical image of a CVD-grown MoS$_2$ flake, which exhibits a uniform ML over its entire surface except for occasional bilayer defects. In order to investigate the effect of photoirradiation in ambient conditions, consecutive PL maps were taken over an area (8.75 μm × 4 μm) marked by a red rectangle in Figure 1b, which includes several areas of interest, i.e., the interior of the MoS$_2$ ML flake, edge of the flake, and Si substrate. Figure 1c shows a typical PL map taken before consecutive photoirradiations. The black dotted box marks the edge region of MoS$_2$.

After taking 20 consecutive PL maps over the area, i.e., after the area was photoirradiated 20 times, the comparison between parts c and d of Figure 1 shows that the PL intensity increased drastically in the edge region. On the other hand, there is almost no change in the PL intensity on the interior of the ML. The total laser radiant exposure is ∼4 mJ/μm^{-2} over 200 s with a measured laser power of 40 μW. The edge region is about 1.5 μm, taking into consideration the laser spot size (∼1.5 μm) of the microscope and the distance (1.25 μm) between pixels. The size of the PL edge region is much larger than the atomic edge of the flake, which is consistent with other reported results obtained using transmission electron microscopy[16] and SNOM.[22]

Parts a and b of Figure 2 show the representative corresponding PL spectra taken on the interior and edge regions measured as a function of the number of laser

Scheme 1. Schematics of the Experimental Setup: *In Situ* Raman Microspectroscopy Equipped with an Environment-Controllable Cell
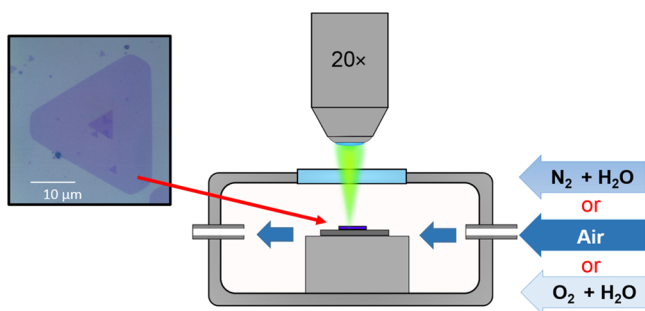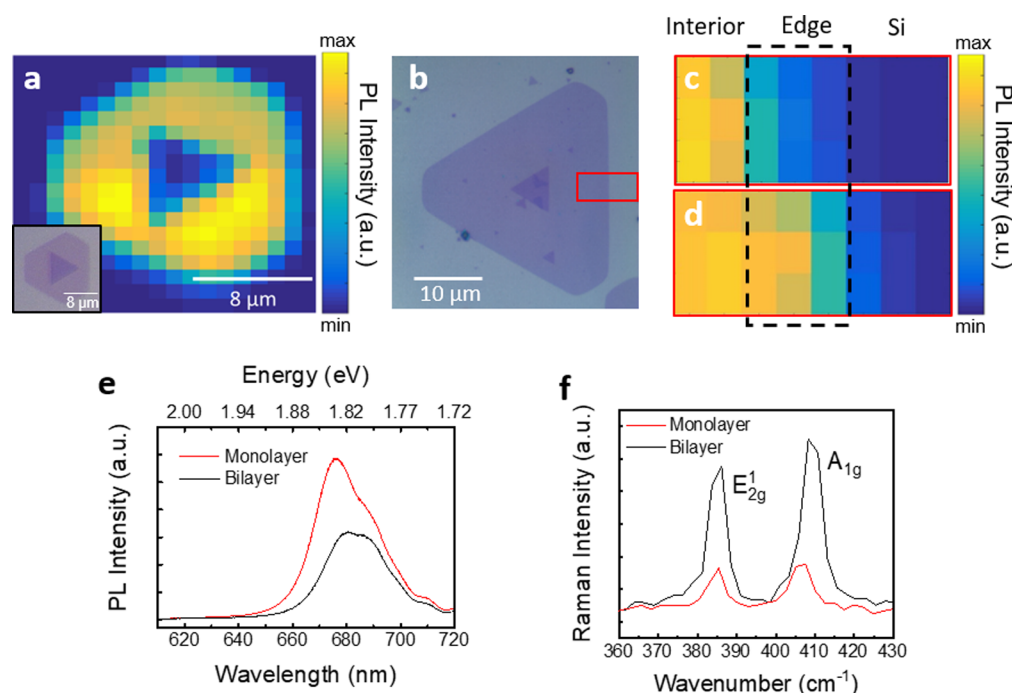
Figure 1. Change of the PL intensity of ML MoS$_2$ with laser irradiation under ambient conditions. (a) PL map of a typical ML MoS$_2$ flake on a SiO$_2$/Si with a bilayer center. Inset: Optical image of the flake mapped in part a. (b) Optical image of a CVD-grown ML MoS$_2$ flake and PL intensity maps taken over the area indicated by the red rectangle before (c) and after (d) ∼20 consecutive photoirradiations. (e) PL and (f) Raman spectra taken from the bilayer and ML of the MoS$_2$ flake in part a, confirming the presence of the ML.

irradiations under ambient conditions. The initial PL near the edge is about 20% of that of the PL on the interior before irradiation. The PL intensity on the interior remains almost constant during photoirradiation under an applied laser power of 40 μW (Figure 2a), but the PL intensity at the edge region increases gradually as a function of the laser irradiation (Figure 2b) until it reaches a saturated PL intensity that is comparable to the PL intensity on the interior. The spectra clearly demonstrate that the PL emission at the edge region is strongly influenced by laser irradiation under ambient conditions.

Statistically, over 50 sets of spectra were taken over the interior of the MoS$_2$ flakes. In the majority of sets (80%), almost no changes in PL were observed. Variation in the 20% could stem from subtle defects on the interior of the MoS$_2$ ML. It has been shown that there is a variation of PL on the MoS$_2$ ML flake.[22] All of the data sets (∼60) taken along the edge of the MoS$_2$ flakes show an increase of the PL. PL maps collected with a smaller laser spot size (∼0.6 μm) and higher laser power of 180 μW show similar results. Further increasing the laser power led to decreasing PL on the interior, which is expected for laser degradation of the flake.[6] Therefore, the laser power was kept at 40 μW for all of the data presented.

There are two reported PL bands from ML MoS$_2$: A exciton at 670 nm (∼1.85 eV) and B exciton at 615 nm (∼2.02 eV).[23] They are associated with direct optical transitions from the lowest conduction bands to the highest spin-split valence bands.[24−26] The A exciton can be deconvoluted into two bands, neutral A^0 exciton and negative A$^-$ multiexciton (biexciton and trion).[27] In our spectra (Figure 2c,d), the A exciton peak is clearly nonsymmetric and shows the existence of multiexcitons. Because the intensity of the B exciton is very small, the spectra are deconvoluted by fitting with two Lorentzian peaks instead of three. We did not distinguish the

biexciton and trion in the analysis and use trion to represent the multiexcitons.

Before consecutive photoirradiations, the shapes of the initial PL spectra for the edge and interior regions are similar, but the intensities of the initial PL are very different (Figures 2c,d). The peak positions of A^0 and A$^-$ on the interior area are 674.8 nm (1.84 eV) and 687.6 nm (1.80 eV), respectively (Figure S2). At the edge region of the MoS$_2$ flake, both peaks are in nearly the same positions as those on the interior. The relative intensity of trion to exciton (Figure 2e,f), i.e., the ratio of the intensity between A$^-$ and A^0, at the edge is 0.4, which is lower than that of 0.6 on the flake interior before irradiation.

Upon photoirradiation, the intensities of both the A$^-$ and A^0 excitons on the interior area (Figure 2e), and the peak positions remain unchanged (Figure S2). At the edge region of the MoS$_2$ flake, the intensity of the A^0 peak increases dramatically (Figure 2f) and approaches the intensity of the interior region. The edge A$^-$ peak intensity also increases appreciably, but it only reaches to about half of that of the interior. Therefore, the ratio of the intensity between A$^-$ and A^0 decreases from 0.4 to 0.3 (Figure 2f). The A^0 peak position has an observable blue shift monotonically from 674.2 nm (1.84 eV) to 671.8 nm (1.85 eV) during photoirradiation, and the A$^-$ peak position stays the same (Figure S2).

The almost constant A^0 and A$^-$ intensities and positions on the interior indicate that there is no detectable defect formation on the surface with a total laser radiant exposure of 4 mJ/μm^{-2} over 200 s. Chow et al. reported a distinct defect-related PL spectral feature located at ∼0.1 eV below the neutral free A^0 exciton peak in WS$_2$ and MoS$_2$ MLs.[28] Our PL spectra do not show that a defect-related PL spectral feature at ∼1.75 eV developed both on the interior and at the edge after irradiation. The optical image of the flake taken after consecutive photoirradiations (Figure 1a) is identical with
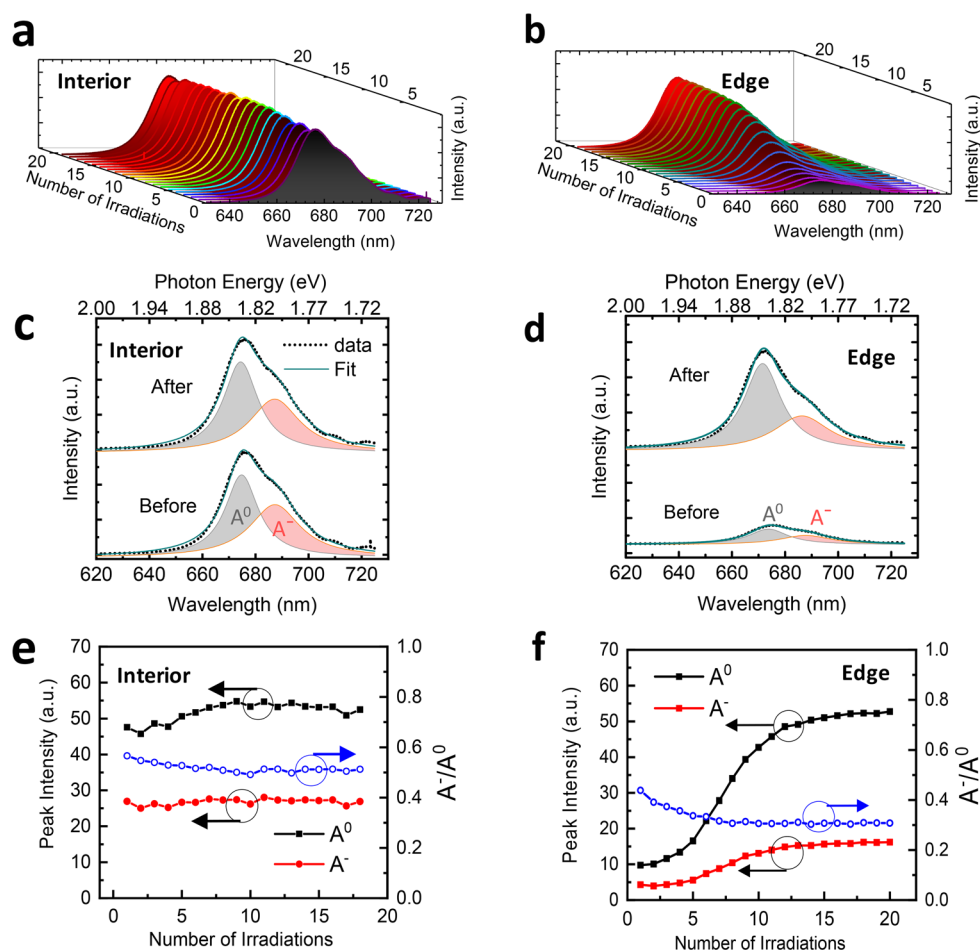
Figure 2. Evolution of PL spectra upon photoirradiation in an ambient environment. PL spectra taken on the interior (a) and edge (b) of a ML MoS$_2$ flake upon consecutive photoirradiations in an ambient environment. The intensity scale in the y axis is the same for parts a and b for comparison. Deconvoluted PL spectra from the interior (c) and edge (d) before and after consecutive photoirradiations. The A exciton emission was deconvoluted into the neutral exciton (A^0) and multiexciton (A$^-$) using Lorentzian curves. Peak intensity (left axis) of the neutral exciton (A^0) and multiexciton (A$^-$) and peak intensity ratio (A$^-$/A^0, right axis) from the interior (e) and edge (f) of MoS$_2$.
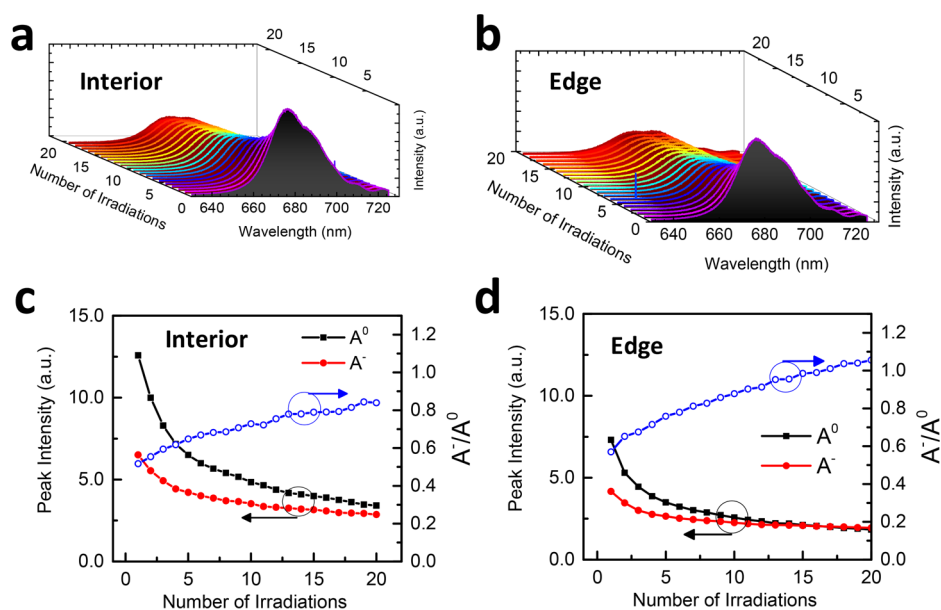

Figure 3. Evolution of PL spectra upon photoirradiation in pure N$_2$. PL spectra taken on the interior (a) and edge (b) of a ML MoS$_2$ flake upon consecutive photoirradiations in N$_2$. Peak intensities (left axis) of neutral exciton (A^0) and multiexiton (A$^-$) and ratio of the peak intensities (A$^-$/A^0, right axis) from the interior (c) and edge (d) of MoS$_2$.
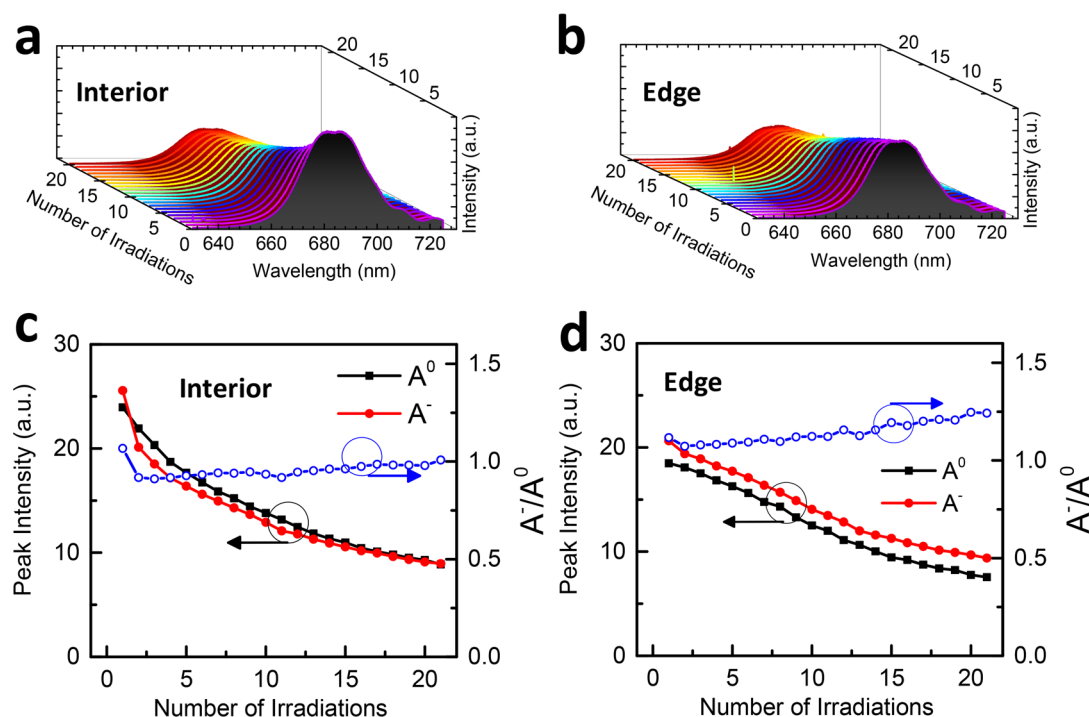
Figure 4. Evolution of PL spectra upon photoirradiation in a H_2O and N_2 mixture. PL spectra taken on the interior (a) and edge (b) of a ML MoS_2 flake upon consecutive photoirradiations in a H_2O and N_2 mixture. Peak intensities (left axis) of neutral exciton (A^0) and multiexiton (A^-) and ratio of the peak intensities (A^-/A^0, right axis) from the interior (c) and edge (d) of MoS_2.
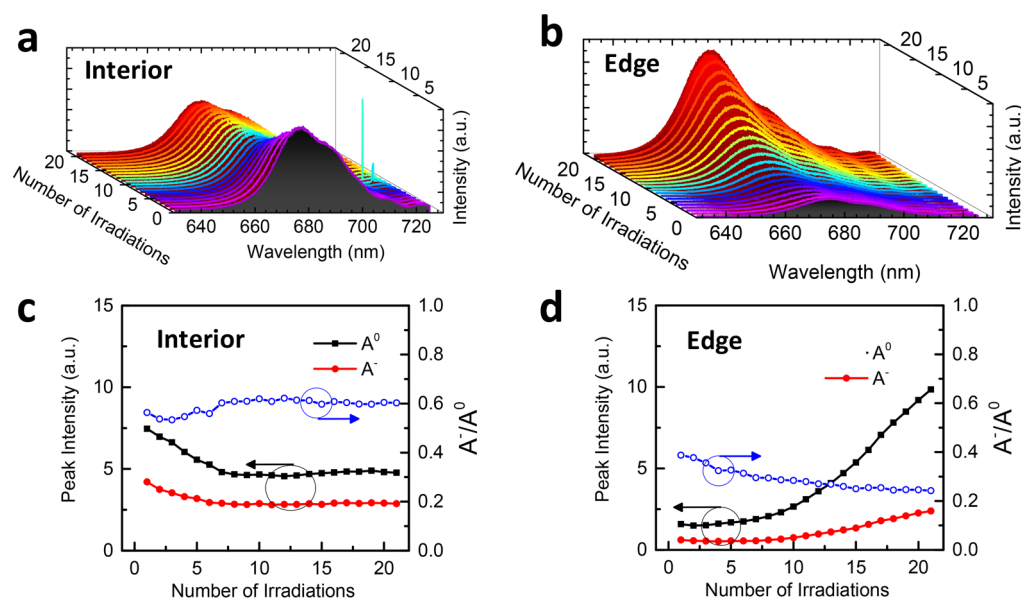

Figure 5. Evolution of PL spectra upon photoirradiation in pure O_2. PL spectra taken on the interior (a) and edge (b) of a ML MoS_2 flake upon consecutive photoirradiations in O_2. Peak intensities (left axis) of neutral exciton (A^0) and multiexiton (A^-) and ratio of the peak intensities (A^-/A^0, right axis) from the interior (c) and edge (d) of MoS_2.

that taken before irradiation, showing no observable photo-damage. AFM images (Figure S1) were acquired on the flakes after photoirradiation. The images include the areas with and without photoirradiation. A direct comparison of these areas shows no detectable structural difference. Raman data (see below) also show that there is no difference before and after photoirradiation in the two MoS_2 modes (E^1_{2g} and A_{1g}). Therefore, the change of the PL at the edge is not due to any discernible structural damage.

It has been reported that the charge-carrier population density affects the line shapes and positions of the PL peaks. Electron doping (n-doping) has been observed to suppress the absorbance of neutral A^0 and enhance the absorbance of trion A^-.[27] The ratio of the intensities between A^- and A^0, i.e., the weight of the A^- trion, has a discernible decrease on the edge, suggesting p-doping due to charge transfer from MoS_2 to adsorbed molecules during photoirradiation. The observed blue shift of the A peak is expected for p-doping,[29] which also supports the p-doping effect during photoirradiation.
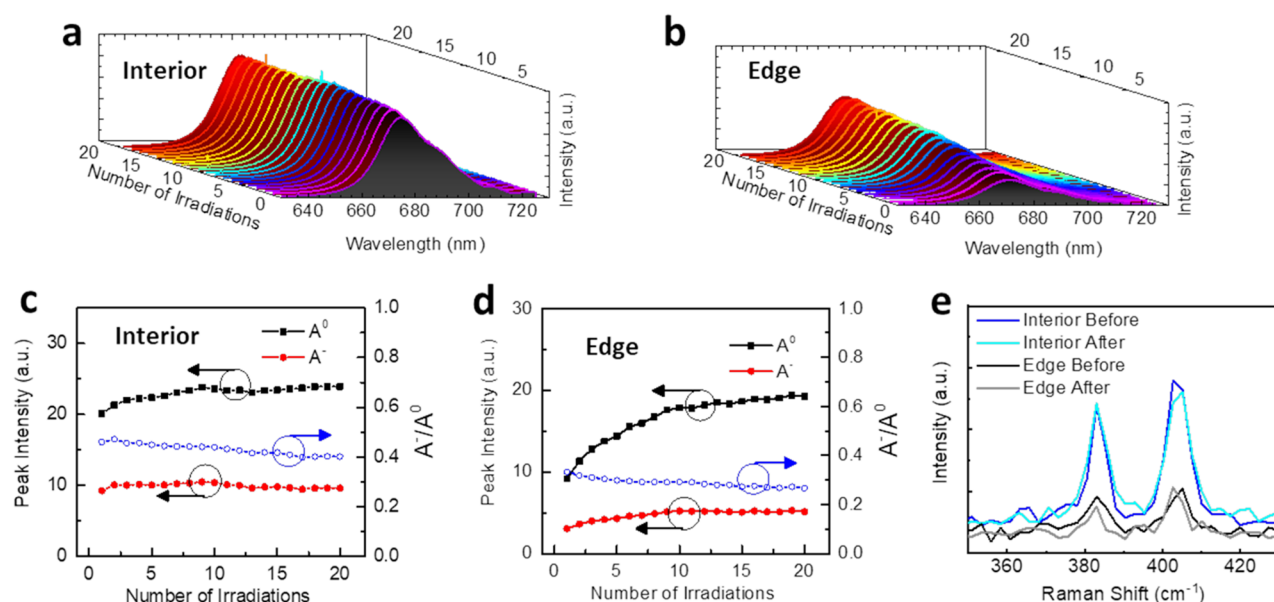
Figure 6. Change of PL and Raman spectra upon photoirradiation in a H_2O and O_2 mixture. PL spectra taken on the interior (a) and edge (b) of a ML MoS_2 flake upon consecutive photoirradiations in a H_2O and O_2 mixture. Peak intensities (left axis) of neutral exciton (A^0) and multiexiton (A^-) and ratio of the peak intensities (A^-/A^0, right axis) from the interior (c) and edge (d) of MoS_2. (e) Raman spectra taken before and after consecutive photoirradiations.

To understand the role of interactions of different molecules with MoS_2 in ambient conditions during photoirradiation, in situ measurements were conducted in an environment-controlled reaction cell in four different gaseous environments, i.e., pure N_2, $H_2O + N_2$, pure O_2, and $H_2O + O_2$. When photoirradiations were conducted in pure N_2, the total PL intensities on both the interior and edge regions decrease monotonically (Figure 3a,b). Deconvolution analysis shows that the intensities of both A^0 and A^- excitons decrease sharply within the first few irradiations and much more slowly with the continued irradiations. Contrary to photoirradiation in ambient conditions, in pure N_2 the weight of A^- increases continuously, indicating an opposite charge-doping process (n-doping).

Adding H_2O vapor to N_2 during photoirradiation did not change the overall trend of the total PL intensity (Figure 4a,b). The total PL intensities on both the interior and edge regions decrease. However, deconvolution analysis shows that the rate of decrease is different in comparison to that in N_2. The intensities of both A^0 and A^- excitons decrease much more slowly than those in N_2, and the intensities of the A^0 and A^- excitons decrease at a similar rate; i.e., the weight of A^- stays almost constant. These observed trends are consistent throughout our samples. This indicates that adding H_2O slows the decrease of PL, which suggests p-doping due to H_2O. There is no change of the peak position for either exciton (Figure S2) in a H_2O and N_2 mixture.

The result of irradiation in pure O_2 (Figure 5) is different from the results obtained in ambient, N_2, and $N_2 + H_2O$. In the interior, the total PL intensity of the A exciton (Figure 5a) and deconvoluted peak intensities of the A^0 and A^- excitons (Figure 5c) had a quick drop during the initial few irradiations and then remain unchanged during subsequent irradiation. This differs from the monotonic decrease observed in the N_2 and $H_2O + N_2$ environments and is also a stark contrast to the unchanged interior PL intensity upon irradiation in air. Further, in O_2, the weight of the A^- peak remains nearly

constant. The initial decreased of PL in O_2 is surprising because p-doping is expected from the adsorption of O_2. This, in fact, reflects the significant role of H_2O that is discussed below.

As for the edge in the O_2 environment (Figure 5b,d), the initial irradiations did not appreciably change the intensities of the A^0 and A^- excitons. Also, there is a continuous increase of intensity for both excitons, unlike in air, where the increasing intensity reaches a plateau. In O_2, the intensity of the A^0 peak continuously increases and reaches an intensity that is even higher than that on the interior before the photoirradiations. The intensity of A^- also continuously increases. The weight of A^- decreases, and there is a blue shift for both A^0 and A^-, indicating p-doping.

Finally, irradiations in the mixture of $H_2O + O_2$ reproduce the trend of the change of the total PL intensity observed in air on both the interior and edge regions. On the interior, the total PL intensity of the A exciton (Figure 6a) and the intensities of deconvoluted A^0 and A^- excitons (Figure 6c) remain almost constant. At the edge, the total PL intensity of the A excitons (Figure 6b) and intensities of deconvoluted A^0 and A^- excitons (Figure 6d) increase continuously, with the total PL intensity reaching a plateau. The difference in the changing rates between exposure in air and in the mixture of $H_2O + O_2$ could relate to the humidity difference between ambient air and the $H_2O + O_2$ environments. There is a blue shift for A^0, which supports p-doping.

Raman spectra can detect the microscopic structural change of ML MoS_2. The Raman spectra were taken before and after photoirradiations in the aforementioned gases to further understand the possible structural change of MoS_2 due to laser irradiation. Figure 6e shows the representative Raman spectra taken in the $H_2O + O_2$ mixture (Figure 6e). Before photoirradiation, at the edge area, the intensities of both the A_{1g} and E_{2g}^1 modes are less than those in the interior. This could be due to disorder of the edge area,[30] which supports that the edge region in synthetic MoS_2 is more complicated

than just its atomic termination and a metallic edge state. An A_{1g} mode peak position shift has been reported due to n-doping in a ML field-effect transistor (FET). Although n-doping is expected for the metallic state of the edge area, the peak positions of both modes are the same as those on the interior. It could be that the doping level is not as high as the doping level in FET resistors.[31] After photoirradiation, there is no discernible change in both the peak positions and intensities on the interior and edge regions (Figure S3). When H_2O intercalation occurs on ML WS_2, Raman spectra show an obvious change in the peak intensity ratio.[12] In the case of photoirradiation-degraded ML MoS_2, the Raman peak intensity and ratio are observed to change.[6] The vibrational modes of MoO_3 are observed on Raman spectra in the process of oxidation of ML MoS_2.[32] This suggests that there is no discernible microscopic structural damage during mild laser irradiation in our results. AFM images (Figure S1) show no detectable structural difference between the areas with and without photoirradiation. However, this does not exclude the creation of atomic point defects.[28,33]

■ DISCUSSION

In ambient conditions before photoirradiation, the PL intensity near the edge is less than that of the PL on the interior. This result agrees with previous reports that the physical and electronic structural difference between the edge and interior strongly affects the PL. Considering that the spatial resolution of Raman spectroscopy applied in this work is diffraction-limited ($\sim$1.5 μm), we show that the disordered edge region is on the order of 1 μm. This is consistent with the reported $\sim$300 nm structural and energetically disordered edge region.[22] Various studies show that the edge of MoS_2 is metallic due to the uncoordinated sites.[34−36] In the presence of high-equilibrium electron density, the probability of forming excitons and trions is expected to rapidly decrease because of electrostatic screening between free electrons and holes.[14] Most of the photoexcited electrons and holes are forced to recombine nonradiatively mostly via the Auger process. Charge screening destabilizes both the excitons and trions; therefore, the PL intensity is low. A similar low PL intensity has been observed for the 1T MoS_2.[20,37] On the other hand, charge accumulation is needed for trions but not for excitons. It would be reasonable to assume that the relative intensity of the trions is higher at the edge because of the high charge density. However, our results show that the relative intensity of the trions is not necessarily higher at the edge region than in the interior. For example, in Figure 1, the relative trion intensity at the edge is 0.44, which is lower than the relative intensity on the interior (0.57) before irradiation. This observation is similar to the observation in nano-PL imaging, which agrees that the edge region is more complicated than a metallic edge state and atomic termination.[22] In our experiments conducted in an ambient environment, both the edge and ML are in air, so there should be physisorbed O_2 and H_2O on both the edge region and the interior of the flake before irradiation. We do not exclude that there could be chemisorbed O_2 and H_2O on the edge before irradiation.

We discuss the effect of photoirradiation on the PL of the interior region first. The PL remains constant upon irradiation in an ambient environment. However, there is a quick decrease during initial irradiations in N_2. This can be attributed to desorption of the physisorbed O_2 and H_2O from the surface during initial irradiations. In air, O_2 and H_2O could readsorb

after photoinduced desorption, and there is no readsorption of O_2 and H_2O in N_2. It has been reported that charge transfer from ideal MoS_2 to physisorbed O_2 (p-doping) is about $\sim$0.02 electrons per molecule.[13,14] Charge transfer from ideal MoS_2 to physisorbed H_2O is also expected (0.01 electrons per H_2O) considering the negatively charged nature of H_2O. On the other hand, N_2 has negligible interaction with ideal MoS_2.[38] The removal of O_2 and H_2O increases the charge density, therefore restoring the charge screening that destabilizes both excitons and trions and drastically decreases the PL upon irradiation in N_2. An increase of the charge density is supported by the increase of the relative trion intensity in N_2 (Figure 3c). Interestingly, irradiation in O_2 alone results in a decrease in PL during the initial photoirradiation (Figure 5a,c). This indicates that adsorption of O_2 alone cannot account for all of the charge transfer from MoS_2 to the adsorbed molecules to keep the PL constant during photoirradiation in air. Our results show that adsorption of both H_2O and O_2 is needed to keep the PL constant (Figure 6a,c). The role of H_2O is supported by the observation that adding H_2O in the N_2 environment significantly slows the rate of decrease of the PL (Figure 4), which suggests that irradiation in H_2O alone most likely would increase the PL due to p-doping. Because PL remains constant during photoirradiation on the interior, it is unlikely that the mild laser power used here introduces additional notable defects. If that was the case, these additional defects would introduce chemisorption of O_2 and H_2O, which would, in turn, change the PL intensity, similar to what was observed on the edge region. The AFM images (Figure S1) support the conclusion that there were no discernible structural changes in the irradiated area. Similarly, mild photoirradiations on ML WS_2 flakes in an ambient environment did not introduce significant change to the PL.[12]

As for the PL at the edge region of MoS_2, there is a drastic increase in PL upon irradiation in ambient conditions and a decrease of PL upon irradiation in N_2. Because physisorbed O_2 and H_2O would be present on both the edge and interior before photoirradiation and the PL of the interior remains unchanged in air, it is unlikely that the drastic increase in PL in the ambient environment is due to the readsorption of physisorbed O_2 and H_2O on the edge region. Otherwise, the PL would remain the same at the edge. The PL intensity drastically increases when irradiation occurs in O_2 (Figure 5b), which suggests that photoirradiation promotes the chemisorption of O_2 molecules at the edge. Nano-Auger microscopy studies reveal that the optically defective grain boundary and edge regions, not just the atomic edge, are S-deficient.[22] Charge transfer from defective MoS_2 to O_2 and H_2O increases dramatically, $\sim$0.6 e per O_2[38] and 0.05 e per H_2O[14] due to interaction of O_2 and H_2O with S vacancies. Charge transfer ($\sim$0.6 e) of the chemisorbed O_2 is much higher than that of physisorbed O_2 ($\sim$0.02 e).[13,38] However, the barrier for chemisorption of O_2 on the S vacancy is $\sim$1 eV.[13] Our results suggest that photoirradiation could assist chemisorption of O_2 and H_2O on the S-vacancy sites in the edge region. Charge transfer reduces the charge accumulated at the metallic edge region and therefore reduces charge screening, which destabilizes both the excitons and trions. This results in a dramatic increase in PL. The decrease of the relative intensity of the trion (Figure 1f) at the edge under ambient conditions is consistent with the reduction of the charge density.

PL loss due to H_2O intercalation has been reported on both MoS_2 and WS_2 flakes on Al_2O_3 substrates. After WS_2 flakes are

briefly exposed to relatively high laser irradiation, the height near the edges of the flakes increases because of H_2O intercalation from the edges and defects.[12,39] The process could also happen after prolonged storage in ambient conditions. AFM images in our study (Figure S1) do not show raised edges, which excludes the contribution of H_2O intercalation.

Upon irradiation in N_2, N_2 could replace physisorbed O_2 and H_2O and adsorb on the S-vacancy sites in the edge region. Different from the negligible charge transfer from ideal MoS_2 to N_2, charge transfer from defective MoS_2 to N_2 is ~0.2 e per molecule.[38] However, the interaction of N_2 with defective MoS_2 is weaker than that of O_2 at defect sites. N_2 drains less electrons (~0.2 e) from the material than O_2 (~0.6 e) via defect sites. Therefore, a decrease in the PL is also observed at the edge region.

$2H$-MoS_2 has two kinds of edges, namely, the Mo- and S-terminated edges.[34−36] The edges of the Mo-terminated $2H$-MoS_2 flakes are metallic[40] and have full S coverage, where each Mo-terminated edge atom has an adsorbed S dimer. The S-terminated edge is bulk-truncated with Mo in its bulk configuration. These edges are the two most energetically stable edge orientations. For the CVD-grown ML MoS_2, the Mo-terminated edges are sharper and straighter than the S-terminated edges. As shown in Figure 1a, our MoS_2 flakes have a rather sharp and straight edge along the side of the triangle, suggesting that the edge type is Mo-terminated on the side of the triangle. The corners of the triangle are not straight, suggesting S-terminated edges. Similar photoirradiation experiments were performed on both Mo- and S-terminated edges in ambient, O_2, N_2, and $H_2O + N_2$. The trends of the change of PL are the same. This is expected from what has been reported from high-resolution scanning transmission electron microscopy studies: that despite the sharp appearance of the edges in optical images, the edges of both the S- and Mo-terminated crystals are rough at the nanoscale.[16]

PL modulation by laser irradiation has been systematically studied and found to be associated with both O_2 and H_2O adsorption as well as laser-induced structural damage.[6] Optical microscopic and AFM images and Raman and PL spectra in our experiments show no structural change on the ML under mild laser power. Therefore, photoinduced chemisorption of H_2O and O_2 to nanoscale defects at the edge region plays a major role in modulation of the PL intensity. Our study shows that, even with mild laser power, the interaction of ambient molecules with defects will largely affect the optical performance of MoS_2 devices. A high-quality ML MoS_2 with few nanoscale defects is critical for MoS_2 optical applications.

CONCLUSIONS

The influence of photochemistry in normal ambient operation conditions on the optical properties of CVD-grown ML MoS_2 has been monitored using *in situ* Raman microspectroscopy. An environment-controllable reaction cell allows us to isolate the effects of various ambient gases by the comparison of photoirradiation in ambient conditions and controlled gaseous environments. The PL intensities of MoS_2 on the interior of ML flakes remain constant upon consecutive photoirradiations in ambient conditions using laser power insufficient to cause structural damage. The PL intensity at the edge region of the synthesized flakes is generally lower than that on the interior but has a dramatic increase upon consecutive photoirradiations in ambient conditions. However, the PL intensities on the interior decrease upon photoirradiations in pure O_2 or N_2, and the adsorption of both H_2O and O_2 molecules is necessary to maintain constant PL intensity. As for the edge region, photoinduced chemisorption of pure O_2 or both H_2O and O_2 increases the PL. Our results provide practical information for applications of MoS_2 devices involving photoirradiation in practical operating conditions, i.e., low laser power in ambient conditions. The optical properties of MoS_2 in a defective area are strongly affected by photoirradiation-induced reactions with O_2 and H_2O.

EXPERIMENTAL METHODS

ML $2H$-MoS_2 flakes were synthesized using the CVD method reported in our previous work.[18] Briefly, an alumina boat containing MoO_3 powder as the growth precursor was placed in the center of the furnace heating zone. A clean SiO_2/Si substrate was placed on top of the boat, with the SiO_2 side facing the precursor. S powder was placed in the upstream zone of the tube furnace. The tube was purged with argon for 15 min, and the growth was maintained at 750 °C for 40 min under the protection of argon. The furnace was then cooled to room temperature naturally.

The CVD-grown MoS_2 sample was exposed to various gases inside an *in situ* reaction cell (Linkam Scientific THMS600) in which the gas flow rate could be finely controlled. Prior to placing the sample in the cell, the cell was baked overnight and then flushed for 5 min independently with targeted gases. Experiments containing water vapor were conducted using a saturator filled with deionized water. The input pure gas (O_2 or N_2) was bubbled through water at a flow rate of 20 mL/min. Prior to photoirradiation, the reaction cell containing the MoS_2 sample was filled with the target gases for several minutes. Air, pure gas, or gas−water mixtures were maintained at a flow rate of 20 mL/min during irradiation.

Photoirradiation was carried out while acquiring PL spectral maps using a Raman microscope. The Raman microscope consisted of a 532 nm laser and a Renishaw inVia Raman spectrometer coupled with a Leica confocal microscope. PL spectra were detected through a 1200 lines/mm grating using continuous rotation to acquire spectra in the 500−725 nm range. Raman spectra were acquired with a stationary grating. All presented MoS_2 PL and Raman spectra were acquired with a 20× oil-based objective with a laser spot size near 1.5 μm directed through a quartz view port on the reaction cell mounted to the Leica microscope. The duration of each laser irradiation at each pixel is 10 s. The applied laser power was kept at 40 μW for all of the presented PL data. The total laser radiant exposure is 4 mJ/μm^{-2} over 200 s. For comparison, PL maps were also collected with a 50× objective with a laser spot diameter near 0.6 μm. The laser power was kept at 180 μW. The total laser radiant exposure was 60 mJ/μm^{-2} over 200 s. AFM images were obtained using a Veeco Dimension 3100 atomic force microscope.

ASSOCIATED CONTENT

Ⓢ Supporting Information

The Supporting Information is available free of charge on the ACS Publications website at DOI: 10.1021/acsanm.8b01422.

AFM image after photoirradiation, evolution of the peak positions of neutral excitons (A^0) and multiexitons (A^-) upon photoirradiation in various gases, and Raman spectra taken before and after photoirradiation (PDF)

AUTHOR INFORMATION

Corresponding Author
*E-mail: Zhenrong_Zhang@baylor.edu.

ORCID ⓘ

Jonathan Hu: 0000-0001-6426-3051
Jun Lou: 0000-0002-0200-3948

Bert M. Weckhuysen: 0000-0001-5245-1426
Zhenrong Zhang: 0000-0003-3969-2326

Notes

■ **REFERENCES**

(1) Bernardi, M.; Palummo, M.; Grossman, J. C. Extraordinary Sunlight Absorption and One Nanometer Thick Photovoltaics Using Two-Dimensional Monolayer Materials. *Nano Lett.* **2013**, *13* (8), 3664−3670.

(2) Chang, K.; Chen, W. L-Cysteine-Assisted Synthesis of Layered MoS_2/Graphene Composites with Excellent Electrochemical Performances for Lithium Ion Batteries. *ACS Nano* **2011**, *5* (6), 4720−4728.

(3) Jariwala, D.; Sangwan, V. K.; Lauhon, L. J.; Marks, T. J.; Hersam, M. C. Emerging Device Applications for Semiconducting Two-Dimensional Transition Metal Dichalcogenides. *ACS Nano* **2014**, *8* (2), 1102−1120.

(4) Ye, G.; Gong, Y.; Lin, J.; Li, B.; He, Y.; Pantelides, S. T.; Zhou, W.; Vajtai, R.; Ajayan, P. M. Defects Engineered Monolayer MoS_2 for Improved Hydrogen Evolution Reaction. *Nano Lett.* **2016**, *16* (2), 1097−1103.

(5) Gutiérrez, O. Y.; Singh, S.; Schachtl, E.; Kim, J.; Kondratieva, E.; Hein, J.; Lercher, J. A. Effects of the Support on the Performance and Promotion of (Ni)MoS_2 Catalysts for Simultaneous Hydrodenitrogenation and Hydrodesulfurization. *ACS Catal.* **2014**, *4* (5), 1487−1499.

(6) Oh, H. M.; Han, G. H.; Kim, H.; Bae, J. J.; Jeong, M. S.; Lee, Y. H. Photochemical Reaction in Monolayer MoS_2 via Correlated Photoluminescence, Raman Spectroscopy, and Atomic Force Microscopy. *ACS Nano* **2016**, *10* (5), 5230−5236.

(7) Mouri, S.; Miyauchi, Y.; Matsuda, K. Tunable Photoluminescence of Monolayer MoS_2 via Chemical Doping. *Nano Lett.* **2013**, *13* (12), 5944−5948.

(8) Ji, Q.; Zhang, Y.; Gao, T.; Zhang, Y.; Ma, D.; Liu, M.; Chen, Y.; Qiao, X.; Tan, P.-H.; Kan, M.; Feng, J.; Sun, Q.; Liu, Z. Epitaxial Monolayer MoS_2 on Mica with Novel Photoluminescence. *Nano Lett.* **2013**, *13* (8), 3870−3877.

(9) Han, H.-V.; Lu, A.-Y.; Lu, L.-S.; Huang, J.-K.; Li, H.; Hsu, C.-L.; Lin, Y.-C.; Chiu, M.-H.; Suenaga, K.; Chu, C.-W.; Kuo, H.-C.; Chang, W.-H.; Li, L.-J.; Shi, Y. Photoluminescence Enhancement and Structure Repairing of Monolayer $MoSe_2$ by Hydrohalic Acid Treatment. *ACS Nano* **2016**, *10* (1), 1454−1461.

(10) Amani, M.; Chin, M. L.; Mazzoni, A. L.; Burke, R. A.; Najmaei, S.; Ajayan, P. M.; Lou, J.; Dubey, M. Growth-Substrate Induced Performance Degradation in Chemically Synthesized Monolayer MoS_2 Field Effect Transistors. *Appl. Phys. Lett.* **2014**, *104* (20), 203506.

(11) Currie, M.; Hanbicki, A. T.; Kioseoglou, G.; Jonker, B. T. Optical Control of Charged Exciton States in Tungsten Disulfide. *Appl. Phys. Lett.* **2015**, *106* (20), 201907.

(12) Atkin, P.; Lau, D. W. M.; Zhang, Q.; Zheng, C.; Berean, K. J.; Field, M. R.; Ou, J. Z.; Cole, I. S.; Daeneke, T.; Kalantar-Zadeh, K. Laser Exposure Induced Alteration of WS_2 Monolayers in the Presence of Ambient Moisture. *2D Mater.* **2018**, *5* (1), 015013.

(13) Nan, H.; Wang, Z.; Wang, W.; Liang, Z.; Lu, Y.; Chen, Q.; He, D.; Tan, P.; Miao, F.; Wang, X.; Wang, J.; Ni, Z. Strong Photoluminescence Enhancement of MoS_2 through Defect Engineering and Oxygen Bonding. *ACS Nano* **2014**, *8* (6), 5738−5745.

(14) Tongay, S.; Zhou, J.; Ataca, C.; Liu, J.; Kang, J. S.; Matthews, T. S.; You, L.; Li, J.; Grossman, J. C.; Wu, J. Broad-Range Modulation of Light Emission in Two-Dimensional Semiconductors by Molecular Physisorption Gating. *Nano Lett.* **2013**, *13* (6), 2831−2836.

(15) Liu, Z.; Amani, M.; Najmaei, S.; Xu, Q.; Zou, X.; Zhou, W.; Yu, T.; Qiu, C.; Birdwell, A. G.; Crowne, F. J.; Vajtai, R.; Yakobson, B. I.; Xia, Z.; Dubey, M.; Ajayan, P. M.; Lou, J. Strain and Structure Heterogeneity in MoS_2 Atomic Layers Grown by Chemical Vapour Deposition. *Nat. Commun.* **2014**, *5*, 5246.

(16) van der Zande, A. M.; Huang, P. Y.; Chenet, D. A.; Berkelbach, T. C.; You, Y.; Lee, G.-H.; Heinz, T. F.; Reichman, D. R.; Muller, D. A.; Hone, J. C. Grains and Grain Boundaries in Highly Crystalline Monolayer Molybdenum Disulphide. *Nat. Mater.* **2013**, *12*, 554−561.

(17) Yin, X.; Ye, Z.; Chenet, D. A.; Ye, Y.; O'Brien, K.; Hone, J. C.; Zhang, X. Edge Nonlinear Optics on a MoS_2 Atomic Monolayer. *Science* **2014**, *344* (6183), 488−490.

(18) Najmaei, S.; Liu, Z.; Zhou, W.; Zou, X.; Shi, G.; Lei, S.; Yakobson, B. I.; Idrobo, J.-C.; Ajayan, P. M.; Lou, J. Vapour Phase Growth and Grain Boundary Structure of Molybdenum Disulphide Atomic Layers. *Nat. Mater.* **2013**, *12*, 754−759.

(19) Zhang, C.; Johnson, A.; Hsu, C.-L.; Li, L.-J.; Shih, C.-K. Direct Imaging of Band Profile in Single Layer MoS_2 on Graphite: Quasiparticle Energy Gap, Metallic Edge States, and Edge Band Bending. *Nano Lett.* **2014**, *14* (5), 2443−2447.

(20) Zhang, J.; Wu, J.; Guo, H.; Chen, W.; Yuan, J.; Martinez, U.; Gupta, G.; Mohite, A.; Ajayan, P. M.; Lou, J. Unveiling Active Sites for the Hydrogen Evolution Reaction on Monolayer MoS_2. *Adv. Mater.* **2017**, *29* (42), 1701955.

(21) Amani, M.; Burke, R. A.; Ji, X.; Zhao, P.; Lien, D.-H.; Taheri, P.; Ahn, G. H.; Kirya, D.; Ager, J. W.; Yablonovitch, E.; Kong, J.; Dubey, M.; Javey, A. High Luminescence Efficiency in MoS_2 Grown by Chemical Vapor Deposition. *ACS Nano* **2016**, *10* (7), 6535−6541.

(22) Bao, W.; Borys, N. J.; Ko, C.; Suh, J.; Fan, W.; Thron, A.; Zhang, Y.; Buyanin, A.; Zhang, J.; Cabrini, S.; Ashby, P. D.; Weber-Bargioni, A.; Tongay, S.; Aloni, S.; Ogletree, D. F.; Wu, J.; Salmeron, M. B.; Schuck, P. J. Visualizing Nanoscale Excitonic Relaxation Properties of Disordered Edges and Grain Boundaries in Monolayer Molybdenum Disulfide. *Nat. Commun.* **2015**, *6*, 7993.

(23) Su, W.; Kumar, N.; Mignuzzi, S.; Crain, J.; Roy, D. Nanoscale Mapping of Excitonic Processes in Single-Layer MoS_2 using Tip-Enhanced Photoluminescence Microscopy. *Nanoscale* **2016**, *8* (20), 10564−10569.

(24) Mak, K. F.; Lee, C.; Hone, J.; Shan, J.; Heinz, T. F. Atomically Thin MoS_2: A New Direct-Gap Semiconductor. *Phys. Rev. Lett.* **2010**, *105* (13), 136805.

(25) Ruckenstein, A. E.; Schmitt-Rink, S. Many-Body Aspects of the Optical Spectra of Bulk and Low-Dimensional Doped Semiconductors. *Phys. Rev. B: Condens. Matter Mater. Phys.* **1987**, *35* (14), 7551−7557.

(26) Splendiani, A.; Sun, L.; Zhang, Y.; Li, T.; Kim, J.; Chim, C.-Y.; Galli, G.; Wang, F. Emerging Photoluminescence in Monolayer MoS_2. *Nano Lett.* **2010**, *10* (4), 1271−1275.

(27) Mak, K. F.; He, K.; Lee, C.; Lee, G. H.; Hone, J.; Heinz, T. F.; Shan, J. Tightly Bound Trions in Monolayer MoS_2. *Nat. Mater.* **2013**, *12*, 207−211.

(28) Chow, P. K.; Jacobs-Gedrim, R. B.; Gao, J.; Lu, T.-M.; Yu, B.; Terrones, H.; Koratkar, N. Defect-Induced Photoluminescence in Monolayer Semiconducting Transition Metal Dichalcogenides. *ACS Nano* **2015**, *9* (2), 1520−1527.

(29) Sim, D. M.; Kim, M.; Yim, S.; Choi, M.-J.; Choi, J.; Yoo, S.; Jung, Y. S. Controlled Doping of Vacancy-Containing Few-Layer MoS_2 via Highly Stable Thiol-Based Molecular Chemisorption. *ACS Nano* **2015**, *9* (12), 12115−12123.

(30) Kang, N.; Paudel, H. P.; Leuenberger, M. N.; Tetard, L.; Khondaker, S. I. Photoluminescence Quenching in Single-Layer MoS_2 via Oxygen Plasma Treatment. *J. Phys. Chem. C* **2014**, *118* (36), 21258−21263.

(31) Chakraborty, B.; Bera, A.; Muthu, D. V. S.; Bhowmick, S.; Waghmare, U. V.; Sood, A. K. Symmetry-Dependent Phonon Renormalization in Monolayer MoS$_2$ Transistor. *Phys. Rev. B: Condens. Matter Mater. Phys.* **2012**, *85* (16), 161403.

(32) Walter, T. N.; Kwok, F.; Simchi, H.; Aldosari, H. M.; Mohney, S. E. Oxidation and Oxidative Vapor-Phase Etching of Few-Layer MoS$_2$. *J. Vac. Sci. Technol., B: Nanotechnol. Microelectron.: Mater., Process., Meas., Phenom.* **2017**, *35* (2), 021203.

(33) Tosun, M.; Chan, L.; Amani, M.; Roy, T.; Ahn, G. H.; Taheri, P.; Carraro, C.; Ager, J. W.; Maboudian, R.; Javey, A. Air-Stable n-Doping of WSe$_2$ by Anion Vacancy Formation with Mild Plasma Treatment. *ACS Nano* **2016**, *10* (7), 6853−6860.

(34) Walton, A. S.; Lauritsen, J. V.; Topsøe, H.; Besenbacher, F. MoS$_2$ Nanoparticle Morphologies in Hydrodesulfurization Catalysis Studied by Scanning Tunneling Microscopy. *J. Catal.* **2013**, *308*, 306−318.

(35) Tuxen, A.; Kibsgaard, J.; Gøbel, H.; Lægsgaard, E.; Topsøe, H.; Lauritsen, J. V.; Besenbacher, F. Size Threshold in the Dibenzothiophene Adsorption on MoS$_2$ Nanoclusters. *ACS Nano* **2010**, *4* (8), 4677−4682.

(36) Lauritsen, J. V.; Kibsgaard, J.; Helveg, S.; Topsøe, H.; Clausen, B. S.; Lægsgaard, E.; Besenbacher, F. Size-Dependent Structure of MoS$_2$ Nanocrystals. *Nat. Nanotechnol.* **2007**, *2*, 53−58.

(37) Voiry, D.; Goswami, A.; Kappera, R.; Silva, C.d.C.C.e.; Kaplan, D.; Fujita, T.; Chen, M.; Asefa, T.; Chhowalla, M. Covalent Functionalization of Monolayered Transition Metal Dichalcogenides by Phase Engineering. *Nat. Chem.* **2015**, *7*, 45−49.

(38) Tongay, S.; Suh, J.; Ataca, C.; Fan, W.; Luce, A.; Kang, J. S.; Liu, J.; Ko, C.; Raghunathanan, R.; Zhou, J.; Ogletree, F.; Li, J.; Grossman, J. C.; Wu, J. Defects Activated Photoluminescence in Two-Dimensional Semiconductors: Interplay Between Bound, Charged, and Free excitons. *Sci. Rep.* **2013**, *3*, 2657.

(39) Zheng, C.; Xu, Z.-Q.; Zhang, Q.; Edmonds, M. T.; Watanabe, K.; Taniguchi, T.; Bao, Q.; Fuhrer, M. S. Profound Effect of Substrate Hydroxylation and Hydration on Electronic and Optical Properties of Monolayer MoS$_2$. *Nano Lett.* **2015**, *15* (5), 3096−3102.

(40) Temel, B.; Tuxen, A. K.; Kibsgaard, J.; Topsøe, N.-Y.; Hinnemann, B.; Knudsen, K. G.; Topsøe, H.; Lauritsen, J. V.; Besenbacher, F. Atomic-Scale Insight Into the Origin of Pyridine Inhibition of MoS$_2$-Based Hydrotreating Catalysts. *J. Catal.* **2010**, *271* (2), 280−289.